Int. J. Heat Mass Transfer. Vol. 34, No. 9, pp. 2303–2315, 1991
Printed in Great Britain

0017–9310/91 $3.00+0.00

A heat flux-meter for ash deposit monitoring systems—II. 'Clean' heat flux-meter characteristics

BRANISLAV BRAJUSKOVIC and NAIM AFGAN
Boris Kidric Institute of Nuclear Sciences, 11 001 Belgrade, Yugoslavia

(*Received* 18 *December* 1989 *and in final form* 26 *October* 1990)

Abstract—The characteristics of a 'clean' heat flux-meter that is air stream cooled and protected against ash deposit formation are presented. The steady state radial temperature difference across the receiving disc of the heat flux-meter is both obtained numerically, using the finite element method, and measured experimentally. Moreover, the steady state receiving disc temperature field circumferential uniformity and the dynamic response of the flux-meter to stepwise changes in the incident heat flux are investigated. The experimental data and numerical results indicate that the radial temperature difference depends linearly on the incident heat flux. The signal vs the air flow rate is also obtained. At steady state conditions and higher air flow rates, the receiving disc temperature field can be considered circumferentially uniform. The dynamic response of the heat flux-meter is satisfactory.

INTRODUCTION

DUE TO the widespread use of low quality coals and their strong tendency to form deposits, reliable and accurate ash deposit monitoring systems are much in demand [1, 2]. Ash deposit formation processes in power plant boiler furnaces are very complex [3–5]. Systems that monitor changes of furnace heat transfer conditions proved to be most efficient and reliable. The major portion of the heat in boiler furnaces is radiation transferred (90–95%) [6]; these systems measure the radiative heat flux. Among the developed monitoring systems [7–9], the one that compares the signals from a so-called 'clean' and a 'dirty' heat flux-meter proved the most reliable. The problem in the development of such a system is the design of a 'clean' heat flux-meter that simulates conditions of heat transfer between the flame and clean furnace walls throughout boiler operation. A 'clean' flux-meter design is proposed in ref. [2]. It has high in-plant positioning flexibility and is efficiently protected against ash deposit formation. In a disc type flux-meter, the heat flux is obtained from the temperature difference between the centre and the perimeter of the receiving disc.

We present experimental data and a numerical evaluation of the dependence of the radial temperature difference across the receiving disc of the proposed 'clean' heat flux-meter on the incident heat flux. Also results of the experimental investigation of the circumferential uniformity of the receiving disc temperature field for steady state radiative heat transfer conditions are shown. The experimental investigation of the dynamic response of the flux-meter to step changes in incident heat flux is discussed.

NUMERICAL EVALUATION OF THE RADIAL TEMPERATURE DIFFERENCE DEPENDENCE ON THE INCIDENT HEAT FLUX

The radial temperature difference dependence on the incident heat flux is determined at steady state heat transfer and two air flow rates (4.6×10^{-3} and 6.8×10^{-3} m^3 s^{-1}). The first step in the determination of the temperature field in the receiving disc is the solution of the steady state Fourier differential equation for conductive heat transfer in cylindrical bodies

$$\frac{\partial^2\Theta}{\partial r^2}+\frac{1}{r}\frac{\partial\Theta}{\partial r}+\frac{\partial^2\Theta}{\partial z^2}=0 \tag{1}$$

$$\Theta(r,z)=t(r,z)-t_0. \tag{2}$$

The prevailing heat transfer conditions and the 'clean' heat flux-meter design (Fig. 1) impose the following assumptions:

(a) radiative and convective heat losses from the lower surface of the receiving disc may be neglected due to the presence of insulation and low air velocities inside the flux-meter housing;

(b) heat conduction losses through the connecting ribs and the influence of the ribs on the circumferential uniformity of the temperature field may be neglected;

(c) heat conduction losses through thermocouple wires (1 mm in diameter) may be neglected.

In view of these assumptions, the boundary conditions become

$$-\lambda(\Theta)\frac{\partial\Theta(r,z)}{\partial z}=q_a-h_1\Theta(r,z);$$

$$z=0,\ 0\leqslant r<R \tag{3}$$

NOMENCLATURE

a	total hemispherical absorptivity
Bi	Biot number
$q_{r,c}$	error due to the different surface temperatures and radiative properties
h_1	coefficient of convective heat transfer from the upper surface of 'clean' heat flux-meter receiving disc
h_2	coefficient of convective heat transfer in the annulus
l	thickness of 'clean' flux-meter receiving disc
n	concentration factor
q	radiation source heat flux
q_a	absorbed heat flux
q_{inc}	incident heat flux
q_{net}	net radiative heat flux
q'	heat flux emitted from receiving discs
R	radius of the receiving disc
S_B	standard error of the linear regression coefficient for $q = A + B(\Delta t)$
$S_{q\|\Delta T}$	standard error of estimate for $q = A + B(\Delta T)$
$S_{q_N\|q_E}$	standard error of estimate for the q_N–q_E regression line
T	temperature
$\dot{V}$	air flow.

Greek symbols

Θ	temperature difference
Ψ	temperature function
δ	thickness
ε	total hemispherical emissivity
λ	coefficient of conductive heat transfer.

Special symbols

ΔT	temperature difference between measuring points
$\mathbb{J}_0$	zero-order Bessel function
$\mathbb{J}_1$	first-order Bessel function.

Subscripts

1–3	temperature measuring points
c	'clean' heat flux-meter
E	experimentally obtained results
N	numerically obtained results
o	environment
s	source
r	referent heat flux-meter.

$$-\lambda(\Theta)\frac{\partial\Theta(r,z)}{\partial r} = h_2\Theta(r,z); \quad 0 < z < 1, r = R \tag{4}$$

$$-\lambda(\Theta)\frac{\partial\Theta(r,z)}{\partial z} = 0; \quad z = 1, 0 \leqslant r < R. \tag{5}$$

The given system of equations (1)–(5) is solved numerically using a two-dimensional heat conduction model for cylindrical bodies [10, 11], based on the finite element method. The convective heat transfer coefficient at the upper surface of the receiving disc, h_1, is calculated using the expression for turbulent flow over the plate. The average v-components of the air velocity above the disc are used to calculate h_1 [2]. The convective heat transfer coefficient in the annulus (air stream outlets), h_2, is calculated using the Roisen–Petuhov expressions [12]. The temperature fields are calculated for incident heat fluxes in the 0–110 kW m^{-2} range and for air flow rates of 4.6×10^{-3} and 6.8×10^{-3} m^3 s^{-1}. The isotherms calculated for an incident heat flux of 100 kW m^{-2} are presented in Fig. 2. The results of temperature field calculations indicate that radial heat transfer is dominant in the receiving disc (Fig. 2). Significant axial heat transfer is limited to the central part of the disc.

The ΔT_{12} radial temperature differences are calculated using the numerically obtained temperatures in the centre and at the periphery of the lower receiving disc surface. Calculated temperature differences ΔT_{12} and the corresponding regression lines for the investigated incident heat flux range and air flow rates are given in Fig. 3. Linear regressions prove to be the best fit for both air flow rates.

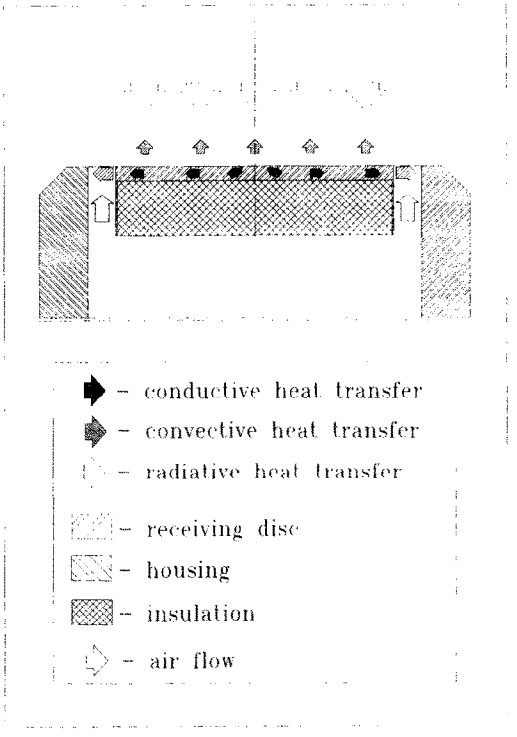

FIG. 1. The 'clean' heat flux-meter—heat transfer conditions.

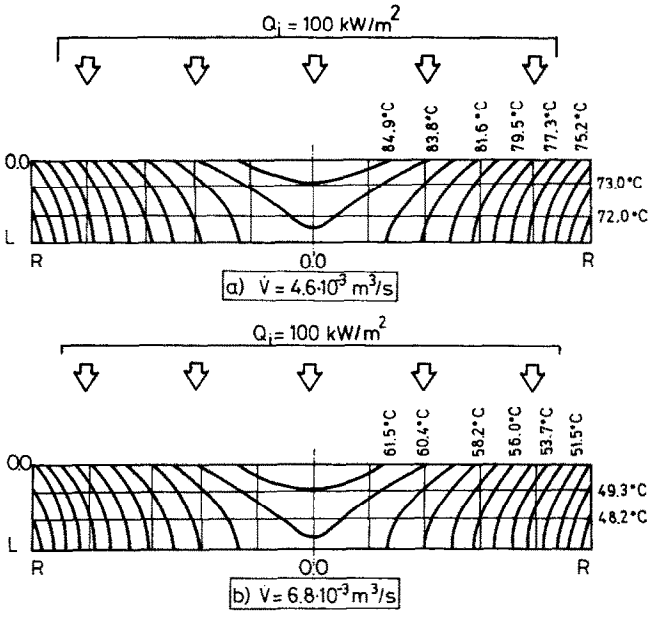

FIG. 2. Temperature field in the receiving disc.

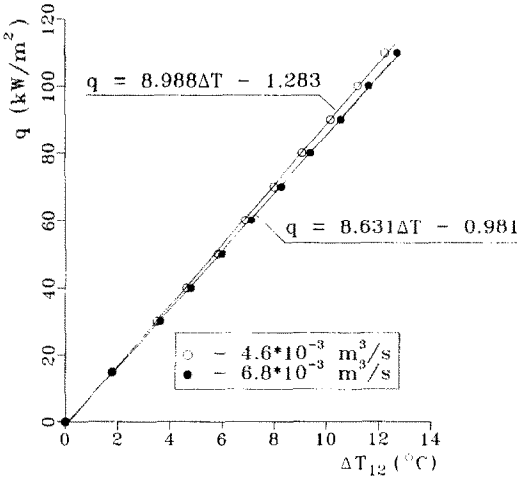

FIG. 3. Numerically obtained radial temperature differences, ΔT_{12}.

Regression line coefficients (A, B), the correlation coefficient (r), the standard error of the estimate ($S_{q|\Delta T}$), the standard error of the regression coefficient B (S_B), and the maximum deviation from regression lines are listed in Table 1. The confidence intervals calculated for 99% probability [13], and intervals of $\pm 2\, S_{q|\Delta T}$ are given in Fig. 3.

It may be seen in Fig. 3 that an increase in the air flow rate results in an increase of the radial temperature difference. A 50% increase in the air flow rate results in a 4.6% increase in the radial temperature difference.

EXPERIMENTAL EVALUATION OF THE 'CLEAN' HEAT FLUX-METER CHARACTERISTICS

Steady state behaviour is experimentally investigated via the radial temperature difference (ΔT_{12}, Fig. 4—detail A) vs incident heat flux dependence and the investigation of the circumferential uniformity of the temperature of the receiving disc. The circumferential uniformity of the temperature field of the receiving disc is investigated by comparing T_2 and T_3 measurements. Steady state characteristics are investigated for an incident heat flux in the 0–105 kW m^{-2} range and for four air flow rates (1.9×10^{-3}, 4.6×10^{-3}, 6.8×10^{-3} and 7.7×10^{-3} m^3 s^{-1}). The heat flux-meter dynamic response to 100% step changes of the incident heat flux is investigated for incident heat fluxes of 60 and 90 kW m^{-2} and at three flow rates (4.6×10^{-3}, 6.8×10^{-3} and 7.7×10^{-3} m^3 h^{-1}).

Experimental set-up

The experimental set-up (Fig. 4) consists of a radiation source (1), a lens radiation concentrator (2), an

Table 1. Statistical parameters—numerical results ($q_N = A + B\Delta T_{N12}$)

$\dot{V}$ (m^3 s^{-1})	Regression coefficients A	B	r	$S_{q\|\Delta T}$ (kW m^{-2})	S_B (kW m^{-2})	Maximum deviation (kW m^{-2})	(%)
4.6E−3	0.801	10.106	0.9996	0.747	0.060	1.283	2.2
6.8E−3	3.066	8.717	0.9997	0.683	0.053	0.950	0.9

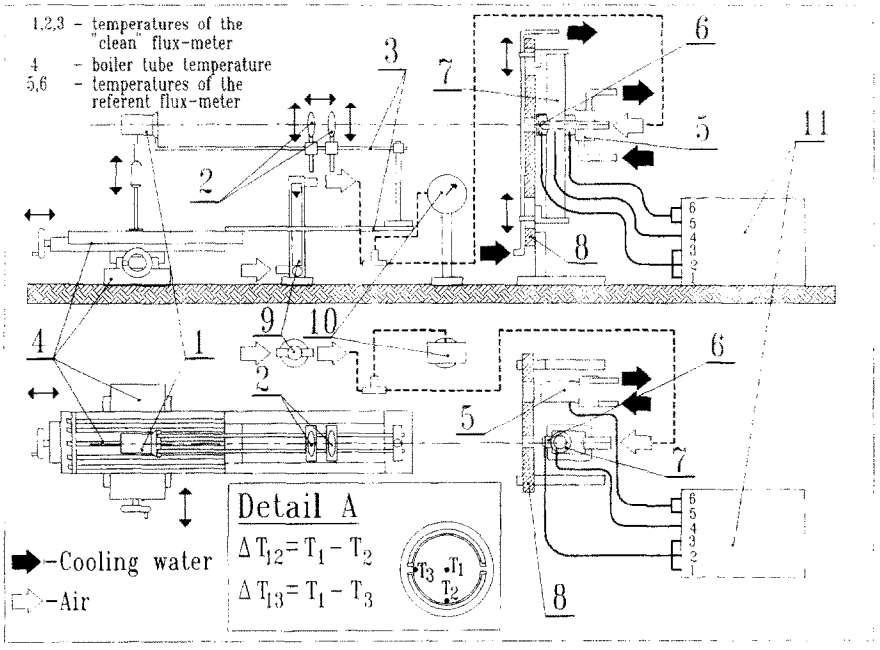

FIG. 4. The experimental set-up.

optical bench (3), a precise positioning system (4), a referent heat flux-meter (5), the investigated 'clean' heat flux-meter (6) fixed to an original boiler tube (7), a water cooled radiation screen (8), the air supply system with flow meter (9) and control manometer (10) and the acquisition system (11).

The radiation source is a Polaris 260 reflector with a 1 kW halogen light source. The reflector has a Fresnel lens and limited collimation. Two converging lenses, 125 mm in diameter and of 400 mm focal length are used for radiation concentration. At the maximum radiation concentration (105 kW m^{-2}, by positioning the lenses along the optical bench) the irradiated area is twice as big as the receiving disc surfaces of both heat flux-meters. The radiation is focused on the receiving discs at angles greater than 80° thus securing the incident heat flux uniformity. The incident heat flux is varied by changing the distance between the radiation source and the flux-meters using a precise positioning system. The precise positioning system ensures identical heat transfer to the referent and 'clean' heat flux-meter. The incident heat flux is measured with a referent flux-meter [14]. Insulated K-type thermocouples are used to measure temperatures in the receiving disc of the 'clean' heat flux-meter. Air flow is controlled by adjusting the valve of a rotameter type laboratory flow meter. An AUTODATA 9 system is used for data acquisition. Step changes in the incident heat flux that induce dynamic response are produced by inserting an 8 mm thick non-transparent plate.

Experimental procedure

Evaluation of the steady state characteristics of the 'clean' heat flux-meter is based on three series of experiments carried out in the mentioned incident heat flux range. First, the incident heat flux was measured using the referent flux-meter, then the 'clean' heat flux-meter was placed in the same position with respect to the radiation source. For each value of the incident heat flux the T_1, T_2 and T_3 temperatures are measured at different air flow rates. Temperatures are measured every 30 s over 5 min intervals at each value of the flow rate. These values were then averaged over the measurement interval. The dependence of the radial temperature difference ΔT_{12} on the incident heat flux was evaluated using the time-averaged values of T_1 and T_2. The time-averaged values of T_2 and T_3 were used to test for circumferential temperature uniformity in the receiving disc.

The 'clean' heat flux-meter dynamic response to the initial incident heat flux is measured in the same manner as the steady state characteristics. After proper positioning of the 'clean' heat flux-meter in respect to the radiation source, a non-transparent 8 mm thick plate is inserted into and removed from the space between the source and the flux-meter and produces incident heat flux step changes. Temperatures were measured until steady state values were reached.

Experimental results

The radial temperature differences, ΔT_{12}, and the obtained correlations for the temperature differences vs the incident heat flux are presented in Figs. 5(a)–(d). The linear regression proves to be the best fit at all air flow rates.

Calculated regression coefficients (A and B), correlation coefficients (r), standard errors of estimate ($S_{q|\Delta T}$), standard errors of the regression coefficient B (S_B) and the maximum deviation of experimental data

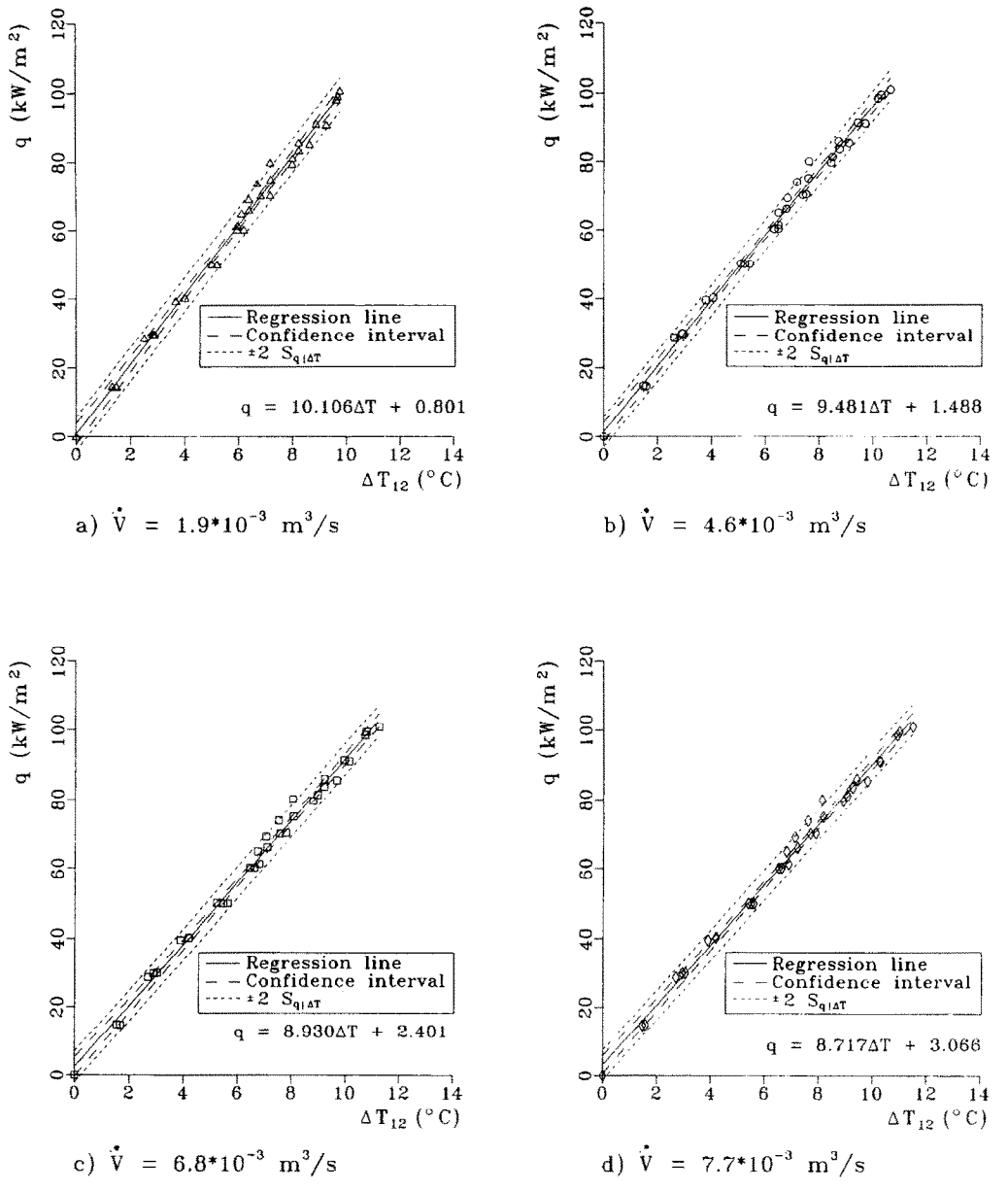

FIG. 5. Experimentally obtained radial temperature differences, ΔT_{12}.

from the corresponding regression lines are listed in Table 2. The confidence intervals (99% probability) and $\pm 2\, S_{q|\Delta T}$ intervals are shown in Figs. 5(a)–(d).

Regression lines obtained for different air flow rates are also presented in Fig. 6. It can be seen that an increase in the air flow rate results in an increase of the ΔT_{12} values obtained at a constant incident heat flux. At the highest incident heat fluxes, a 300% increase in the air flow rate results in a 13.5% increase of the temperature difference.

The results of the T_2 and T_3 measurements are shown in Figs. 7(a)–(d). Note a small temperature difference for different positions on the receiving disc perimeter for all incident heat fluxes. As the incident heat flux increases, the circumferential temperature difference, ΔT_{23} (Fig. 4—detail A), also increases until the incident heat flux reaches the 85–90 kW m^{-2} range. On further increasing of the incident heat flux, the temperature difference ΔT_{23} decreases. With the increase of the air flow rate, the observed circumferential temperature differences decrease.

The flux-meter signals upon a 100% step decrease and subsequent increase of incident heat flux are presented in Figs. 8(a)–(d). After the step incident heat flux decrease the 'clean' heat flux-meter signals reach steady state values after, at most, 18 s. With the increase

Table 2. Statistical parameters—experimental results ($q_E = A + B\Delta T_{E12}$)

$\dot{V}$ ($m^3 s^{-1}$)	Regression coefficients A	B	r	$S_{q\|\Delta T}$ (kW m^{-2})	S_B (kW m^{-2})	Maximum deviation (kW m^{-2})	(%)
1.9E−3	0.801	10.106	0.9917	2.465	0.169	6.485	8.1
4.6E−3	1.488	9.481	0.9934	2.193	0.141	6.406	8.0
6.8E−3	2.401	8.930	0.9936	2.261	0.137	5.661	7.1
7.7E−3	3.066	8.717	0.9936	2.166	0.128	5.929	7.4

in the incident heat flux this time interval lengthens. On the other hand, the increase of the air flow rate shortens this time interval. For the step heat flux increase, flux-meter signals reach stable values after a maximum of 14 s. A subsequent increase of the incident heat flux again increases the time interval needed for the signals to stabilize. At the beginning of the measurement sudden peaks of the signal were noticed at step decreases of the incident heat flux. Also, at step heat flux increases, negative values of flux-meter signals were observed at the beginning of the measurement.

The time constants of the 'clean' heat flux-meter, calculated using the experimentally obtained responses of the flux-meter to step changes in the incident heat flux, are given in Table 3. For all the investigated cases, the calculated time constants are shorter than 5 s. The longest time constant (4.6 s) was obtained for the 100% step decrease from a 60 kW m^{-2} incident heat flux initial value and at a 6.8×10^{-3} $m^3 s^{-1}$ air flow rate. The lowest value of the time constant (2.33 s) was obtained for the incident heat flux step increase from 0 to 90 kW m^{-2} and an air flow rate of 6.8×10^{-3} $m^3 s^{-1}$.

The data presented in Table 3 shows that at a step decrease, time constant values tend to decrease with the increase in the air flow rate. The increase in the initial incident heat flux results in an increase in the time constant values except for the air flow rate of 6.8×10^{-3} $m^3 s^{-1}$ where a 50% increase in the incident heat flux produces a 11.5% decrease in the time constant. At a step increase of the incident heat flux, an increase in the air flow rate results in an increase in the time constant values except for a 90 kW m^{-2} incident heat flux and air flow rates of 4.6×10^{-3}–6.8×10^{-3} $m^3 s^{-1}$ where a 47.8% increase in the air flow rate produces a 45.5% decrease in the value of the time constant. The increase in the initial incident heat flux causes, in the case of a step increase, a decrease in the value of the time constant except for an air flow rate of 4.6×10^{-3} $m^3 s^{-1}$ where a 50% increase in the incident heat flux produces a 59.9% increase in the value of the time constant.

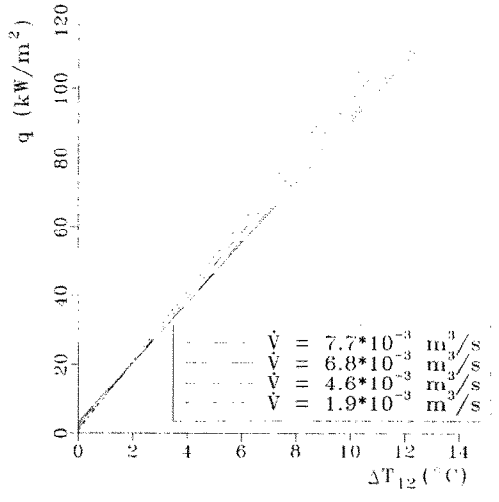

FIG. 6. Experimentally obtained correlations, $q = f(\Delta T_{12})$.

DISCUSSION

Numerically obtained dependence of the radial temperature difference on the incident heat flux

The linear regression best fits the numerically evaluated dependence of the radial temperature differences on the incident heat flux in the receiving disc of the 'clean' heat flux-meter. Corresponding correlation coefficients are very close to 1 and the standard errors of estimate do not exceed 0.75 kW m^{-2} for both air flow rates. The observed dependence of ΔT_{12} on the air flow rate where, for instance, at the highest values of the incident heat flux, a 1% increase in air flow rate results in approximately a 0.09% increase in the radial temperature difference, is in good agreement with the numerical solution for the radial temperature difference between the centre and perimeter of the lower receiving disc surface. The temperatures in the centre and at the periphery of the lower surface of a cylindrical body, for boundary conditions (3)–(5), are [14]

$$\Psi(0,1) = \frac{q_{net}R^2}{4\lambda_0\delta}\sum_{k=1}^{\infty}\frac{8\frac{1}{R}\mathbb{J}_1(\omega_k)}{\omega_k^2\cosh\left(\omega_k\frac{1}{R}\right)[\mathbb{J}_0^2(\omega_k)+\mathbb{J}_1^2(\omega_k)]} \quad (6)$$

$$\Psi(R,1) = \frac{q_{net}R^2}{4\lambda_0\delta}\sum_{k=1}^{\infty}\frac{8\frac{1}{R}Bi}{\omega_k(\omega_k^2+Bi^2)\cosh\left(\omega_k\frac{1}{R}\right)} \quad (7)$$

where

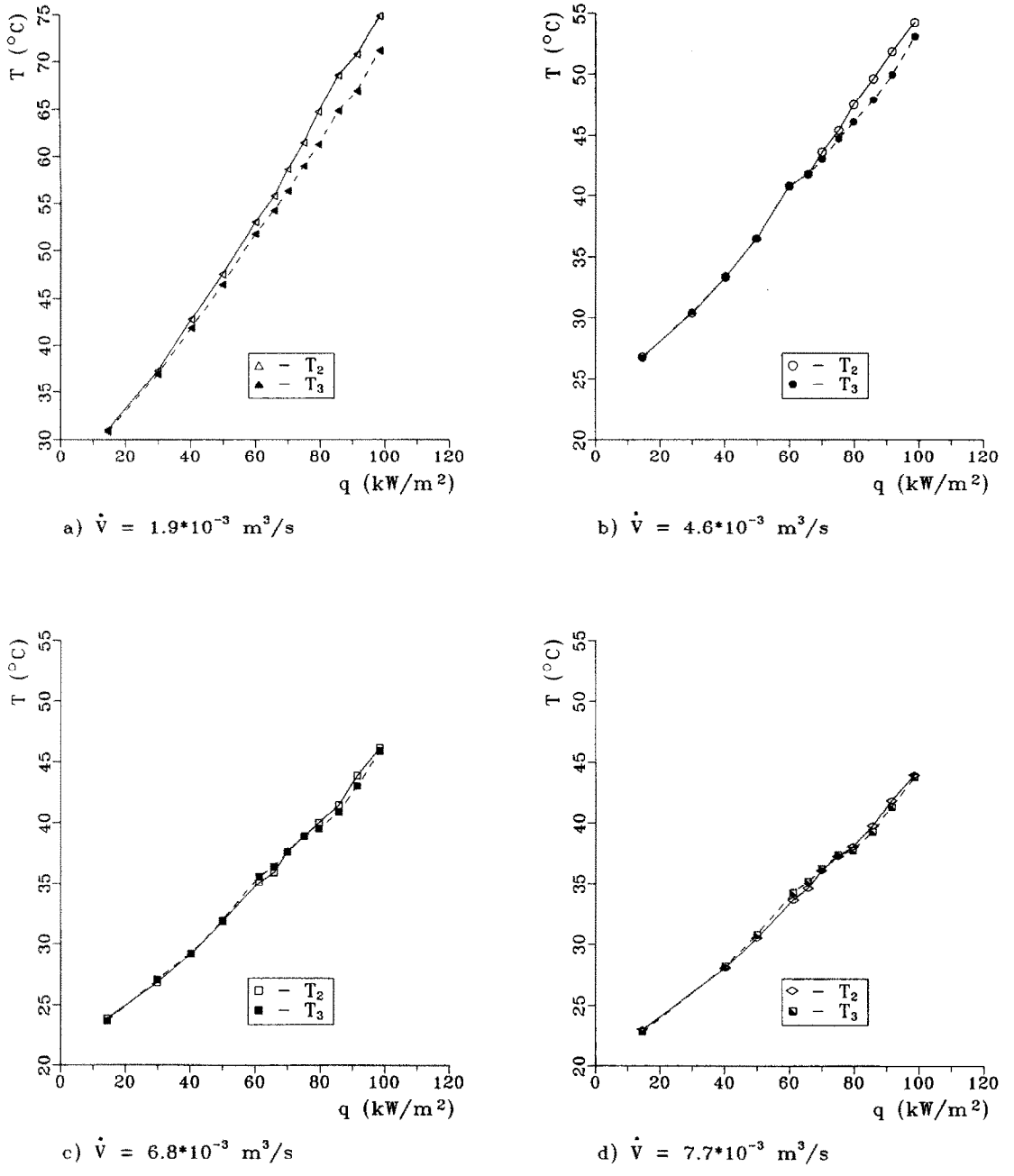

FIG. 7. Temperatures at the periphery of the receiving disc.

$$q_{\text{net}}(r,0) = a_c q_{\text{inc}} - h_1(r,0) \tag{8}$$

$$\Psi(r,z) = \frac{1}{\lambda_0}\int_0^{\Theta} \lambda(\Theta)\,\mathrm{d}\Theta. \tag{9}$$

A temperature function (9) is introduced to simplify the solution of the system of equations (1)–(5) [14, 15]. The expression for the radial temperature difference at the lower surface of the receiving disc can be derived from equations (6) and (7)

$$\Delta\Psi = \Psi(0,1) - \Psi(R,1)$$

$$= \frac{q_{\text{net}} R^2}{4\lambda_0\delta} \sum_{k=1}^{\infty} \frac{8\dfrac{1}{R}}{\omega_k \cosh\left(\omega_k \dfrac{1}{R}\right)} \left[\frac{\mathbb{J}_1(\omega_k)}{\omega_k[\mathbb{J}_0^2(\omega_k) + \mathbb{J}_1^2(\omega_k)]} - \frac{Bi}{(\omega_k^2 + Bi^2)} \right]. \tag{10}$$

Equation (10) indicates that an increase in the flow

rate and thus an increase of Bi results in an increase in the radial temperature difference at the lower surface of the receiving disc.

During the numerical evaluation of the radial temperature difference vs incident heat flux dependence several possible sources of error were identified:

(a) the error inherent in the numerical method itself;

(b) the error introduced via material thermo-physical properties used in the calculation;

(c) the error due to the calculated convective heat transfer coefficients h_1 and h_2;

(d) the error that is the result of neglecting the conductive heat losses through the connecting ribs and thermocouple wires and convective and radiative heat losses from the lower surface of the receiving disc.

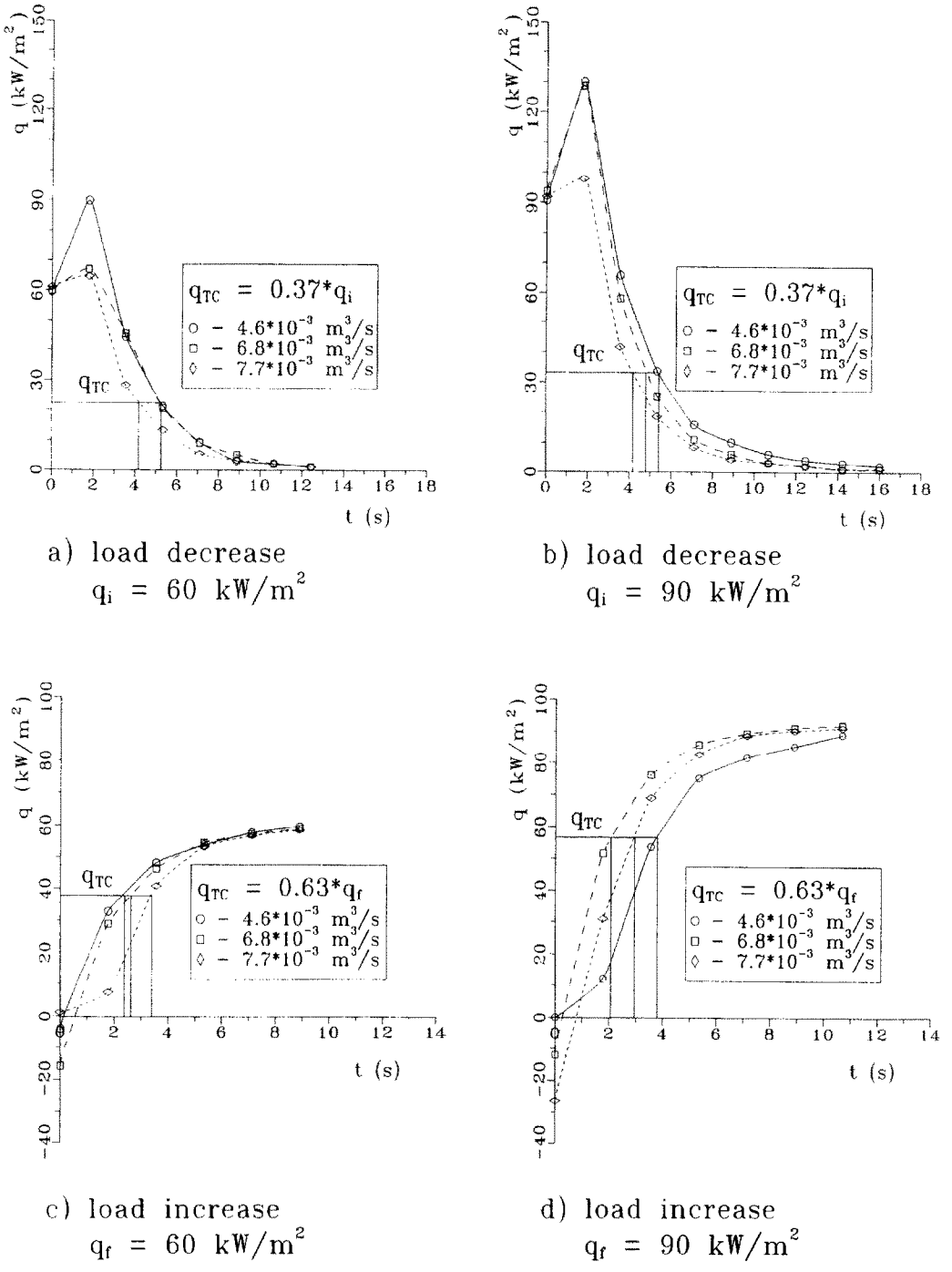

FIG. 8. Dynamic response of the 'clean' heat flux-meter.

Table 3. Time constants of the 'clean' heat flux-meter

Q (kW m^{-2})	Time constant (s) $\dot{V} = 4.6\times10^{-3}$ m^3 s^{-1}	$\dot{V} = 6.8\times10^{-3}$ m^3 s^{-1}	$\dot{V} = 7.7\times10^{-3}$ m^3 s^{-1}
Step decrease of the incident heat flux			
60	4.47	4.59	3.45
90	4.52	4.06	3.47
Step increase of the incident heat flux			
60	2.67	2.95	3.82
90	4.27	2.33	3.32

The chosen non-uniform numerical grid proved optimal in terms of numerical stability and run time of the temperature field computation [10, 11]. It minimizes the error inherent in the numerical method itself. All thermo-physical property values are taken from the literature [16–18]. The cross-section ratios of the receiving disc surface and the connecting ribs and thermocouple wires are such that the heat losses through the connecting ribs and thermocouple wires do not considerably affect the accuracy of the evaluation of the ΔT_{12} dependence on the incident heat flux at steady state. Also, due to the insulating layer, convective heat losses at the rear surface of the receiving disc are negligible.

In the calculation of the h_1 convective heat transfer coefficient average values of the experimentally obtained v-component of air velocity are used [2]. The v-component values of air velocity are several times greater at the perimeter than at the centre of the receiving disc. The nonuniformity of the air velocities indicates that convective heat transfer from the upper surface of the receiving disc is also nonuniform, contrary to the assumption we made in our attempt to simplify the numerical solution. Furthermore, due to the dimensions of the 'clean' heat flux-meter, air flow instabilities in the annulus may be expected to contribute to the error in the numerical evaluation of the mentioned dependence. The only plausible quantification of the error in the numerical evaluation of the steady state ΔT_{12} dependence on the incident heat flux due to the calculated h_1 and h_2 values is by comparison with experimental data.

Experimental radial temperature difference vs incident heat flux curves

Linear regressions are the best fit for the ΔT_{12} radial temperature difference vs incident heat flux data obtained at all investigated flow rates. Obtained correlation coefficients are in the range of 0.992–0.994 and the standard errors of estimate do not exceed 2.5 kW m^{-2}. The lowest values of the correlation coefficient and the highest values of the standard error of estimate are at the lowest air flow rate (1.9×10^{-3} m^3 s^{-1}). The radial temperature difference vs air flow rate dependence observed is virtually equal to the numerically obtained results. In the air flow range of 4.6×10^{-3}–6.8×10^{-3} m^3 s^{-1}, a 1% increase in the air flow rate results in a 0.1% increase in the radial temperature difference. As air flow rate instabilities in an actual power plant boiler environment can be controlled to less than $\pm10\%$ it is reasonable to expect that 'clean' heat flux-meter signal variations due to air flow rate changes do not exceed $\pm1\%$ of the mean value.

The principal potential sources of error in the experimental evaluation of ΔT_{12} vs incident heat flux dependence are:

(a) referent and 'clean' flux-meter receiving disc surface different radiative properties;
(b) referent and 'clean' heat flux-meter surface temperature discrepancies;
(c) temperature measurement errors;
(d) the error in determination of the actual distance between the attached thermocouples.

The error in the experimental evaluation of the ΔT_{12} dependence on the incident heat flux due to the different radiative properties and surface temperatures is obtained from

$$g_{r,c} = \frac{q_{r,net} - q_{c,net}}{q_{r,net}}. \tag{11}$$

The net radiative fluxes between the radiation source and receiving discs of the referent and 'clean' heat flux-meter are

$$q_{r,net} = q_r - q'_r = \sigma(na_r\varepsilon_s T_s^4 - \varepsilon_r T_r^4) \tag{12}$$

$$q_{c,net} = q_c - q'_c = \sigma(na_c\varepsilon_s T_s^4 - \varepsilon_c T_c^4). \tag{13}$$

Equation (11) becomes

$$g_{r,c} = \frac{\sigma(na_r\varepsilon_s T_s^4 - \varepsilon_r T_r^4) - \sigma(na_c\varepsilon_s T_s^4 - \varepsilon_c T_c^4)}{\sigma(na_r\varepsilon_s T_s^4 - \varepsilon_r T_r^4)}. \tag{14}$$

During the experimental evaluation of the ΔT_{12} dependence on the incident heat flux we monitored the referent flux-meter receiving disc surface temperature. The obtained data show that both flux-meter surface temperatures do not exceed 400 K and that the difference between them does not exceed 20 K. Since the temperature of the light source is 3000 K, all the terms in equation (14) containing T_r or T_c can be neglected reducing it to

$$g_{r,c} = \frac{\sigma n\varepsilon_s T_s^4(a_r - a_c)}{\sigma n a_r\varepsilon_s T_s^4} = \frac{a_r - a_c}{a_r}. \tag{15}$$

Equation (15) indicates that the error in the evaluation of the ΔT_{12} vs incident heat flux dependence is strongly influenced by the difference in total hemispherical absorptivity values. The referent heat flux-meter is coated with a temperature resistant black paint of a total hemispherical absorptivity of $a_r = 0.9$, the total hemispherical absorptivity for the stainless steel surface of the 'clean' flux-meter being approximately $a_c = 0.4$ [16, 18]. The error due to this difference in radiative properties is 45%. In an attempt to diminish the effect of receiving disc surface radiative properties on the accuracy of the experimental evaluation of ΔT_{12} vs the incident heat flux, the measured radial temperature differences are related not to the absorbed but to the incident heat flux. Thus, any serious repercussions of the different radiative properties and surface temperatures are eliminated.

As mentioned above, temperatures are measured with insulated K-type thermocouples. As calibrated thermocouples are used, the error introduced by the thermocouples may be neglected. The accuracy of the voltmeter is 1%. The measured temperatures are processed with one significant decimal digit resulting in ± 7.4 and $\pm 0.8\%$ errors for the lowest and highest values of radial temperature differences, respectively. The total temperature measurement error is $\pm 8.5\%$ for the lowest incident heat flux and air flow rate values and $\pm 1.8\%$ for the highest incident heat flux and air flow rates.

At receiving disc and thermocouple diameters of 10 and 1 mm, respectively, the displacement of each thermocouple from the intended position may be expected not to exceed 0.1 mm. Due to the unique flux-meter design (a 0.1 mm thick metal wall used for attaching the insulation prevents the displacement of the perimeter thermocouple in that direction) a -0.2 to 0.1 mm total positioning error for both thermocouples may be expected. The results of the temperature field calculations indicate (Fig. 2) that, due to nonuniformity of the radial temperature gradient, a central thermocouple displacement affects the accuracy less than displacement of the perimeter thermocouple. An analysis of the temperature field calculations and possible thermocouple positions indicates that the error due to the displacement of thermocouples should not exceed -2.9 and -2.6% for the lowest and the highest incident heat fluxes and air flow rates, respectively.

In accordance with the above analysis of the main sources of error in the experimental evaluation of the ΔT_{12} vs incident heat flux dependence, it is to be expected that the total error does not exceed -11.2 to 8.5% for the lowest values of incident heat flux and air flow rate and -4.5 to 1.8% for the highest values.

Comparison between experimental and numerical results

Linear correlations of the ΔT_{12} radial temperature differences and incident heat flux proved the best in both the experimental and numerical investigations. Experimental incident heat flux data (q_E) and the computed incident heat flux values obtained for similar radial temperature differences using the numerical correlations (q_N) are given in Fig. 9. In the 15–105 kW m^{-2} incident heat flux range, the average differences between numerically and experimentally obtained values are 3.3 and 5.0% for airflow rates of 4.6×10^{-3} and 6.8×10^{-3} m^3 s^{-1}, respectively. The greatest differences between numerically and experimentally obtained heat flux are 8.9 kW m^{-2} (12.5%) for the lower and 10.6 kW m^{-2} (15.3%) for the higher air flow rate.

At similar incident heat fluxes and air flow rates the experimentally obtained ΔT_{12} values are lower than those obtained numerically (Figs. 3, 5 and 9). The influence of the air flow rate increase on the radial temperature difference is slightly more significant in the case of experimental flux-meter characteristics. For the highest values of the incident heat flux a 1% increase of the air flow rate in the 4.6×10^{-3}–6.8×10^{-3} m^3 s^{-1} range results in 0.1 and 0.09% increases in the radial temperature differences according to the experimental and the numerical evaluations, respectively.

The slopes of the q_E–q_N regression lines differ from

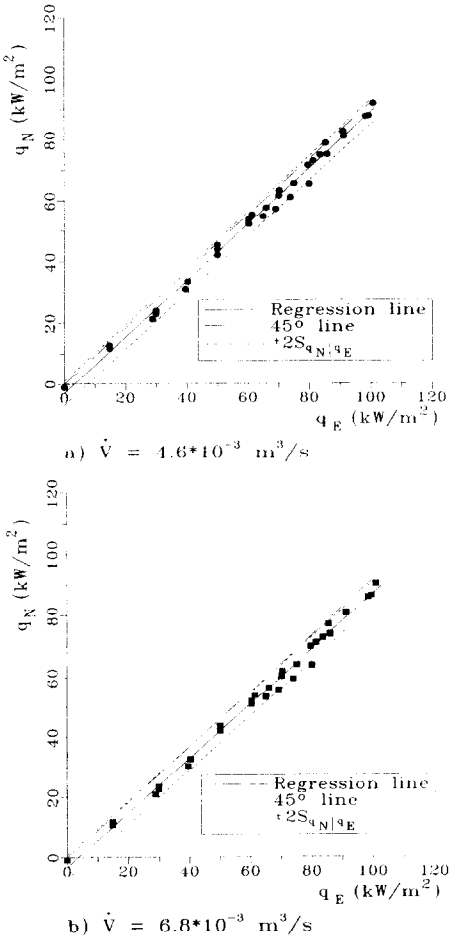

FIG. 9. Comparison between experimental and numerical data.

45° less than 1′ for the lower and 28′ for the higher air flow rate indicating that the difference between experimental and numerical data is virtually constant for all incident heat fluxes. These differences are mainly due to the disagreement in the total hemispherical absorptance value used in the numerical evaluation and the actual value. The convective heat transfer nonuniformity due to the velocity profile and possible flow instabilities contribute to the dispersion of regression line slopes around 45°. As mentioned, because slope dispersion is smaller than 30′, the influence of the convective heat transfer instabilities at the upper surface of the receiving disc may be neglected.

The analysis of experimental error limits shows that the numerical data lie within, or are close to, the experimental error limits indicating that the 'clean' flux-meter can be successfully numerically calibrated. Note that, since in the 4.6×10^{-3}–6.8×10^{-3} m^3 s^{-1} air flow range, the mean values of the v-component of air velocity data vary little with the change of the air flow rate [1], the developed numerical model can be used for the calibration of the 'clean' heat flux-meter in the air flow rate range in question without the need for additional velocity field measurements.

Circumferential temperature field uniformity

The results of T_2 and T_3 measurements indicate that the increase of incident heat flux up to 85–90 kW m^{-2} results in an increase in the circumferential temperature difference. At higher incident heat fluxes circumferential temperature differences decrease with the increase in the incident heat flux. It may be seen in Figs. 7(a)–(d) that up to an incident heat flux of 85–90 kW m^{-2}, the T_2 temperature rises faster than T_3. At higher values of the incident heat flux, the opposite occurs. This is due to the relationship between the temperatures of the flux-meter housing and the receiving disc. If the temperature of the housing is lower than the temperature of the receiving disc, the connecting ribs act as a heat sink, increasing the heat transfer rate. Once the temperature of the housing becomes higher than that of the receiving disc, the connecting ribs begin to act as heat sources. Obtained results indicate that for incident heat fluxes above 85–90 kW m^{-2}, the temperature of the housing exceeds the temperature of the receiving disc due to less efficient cooling and the connecting ribs cease to increase the heat transfer rate.

An increase in the air flow rate reduces circumferential temperature differences. At a flow rate of 7.7×10^{-3} m^3 s^{-1} circumferential temperature differences almost disappear. The reduction of the circumferential temperature differences with the increase in the air flow rate is due to the increased efficiency of convective cooling of the receiving disk.

The highest circumferential temperature differences were measured at a 90 kW m^{-2} incident heat flux. The observed circumferential temperature distribution results in radial temperature differences ΔT_{12} and ΔT_{13} (Fig. 4—detail A) of 40.9% at 6.8 m^3 h^{-1} to 4.8% at 27.7 m^3 h^{-1}. In view of the geometry of the receiving disc and the obtained results, the influence of the connecting ribs on the temperature field of the receiving disc is, at higher air flow rates, limited to their vicinity. The circumferential thermocouple displacement at air flow rates of 4.6×10^{-3} m^3 s^{-1} and higher does not affect the accuracy of the measurement.

The dynamic response of the 'clean' heat flux-meter

The dynamic response of the 'clean' heat flux-meter was experimentally investigated for two values of the incident heat flux of 60 and 90 kW m^{-2}. The results indicate that the flux-meter signal stabilizes in no longer than 18 s after a 100% step decrease and 14 s after a 100% step increase of incident heat flux. The value of incident heat flux of 90 kW m^{-2} used in the experiments is close to that expected in the boiler furnace zone where the 'clean' heat flux-meter will be mounted (incident heat fluxes in boilers fired with pulverized low quality lignites in the above-burner zone are in the 100–125 kW m^{-2} range [19]). Comparison of the 'clean' heat flux-meter dynamic characteristics and the dynamics of boiler furnace processes indicates that the 'clean' heat flux-meter will register all incident heat flux oscillations that are of interest to ash fouling monitoring systems.

During the evaluation of the dynamic response of the 'clean' heat flux-meter, the peaks and negative values of the flux-meter signal were observed during the first 2 s. Heat is transferred by conduction through the receiving disc almost instantaneously (the conduction heat transfer rate in temperature resistant steels is estimated in the 350–400 m s^{-1} range [20]) and the observed phenomena are due to heat transfer through the receiving disc (Fig. 2). After a stepwise decrease in the incident heat flux, temperatures decrease more slowly at the centre of the lower surface of the receiving disc than at the periphery resulting in higher radial temperature differences and an increase in the flux-meter signal. This is due to axial heat transfer from the upper surface of the receiving disc to the colder lower surface. In the case of a step increase in the incident heat flux, heat is transferred from the upper surface of the receiving disc more intensively in the radial direction thus inducing a faster increase of periphery temperatures than those at the centre of the lower surface of the receiving disc.

The calculated values of the 'clean' heat flux-meter time constant (Table 3) indicate that for incident heat flux decreases, the time constant shortens with the increase in the air flow rate and the decrease in the incident heat flux. The influence of the air flow rate on the time constant is considerably more pronounced than the influence of the incident heat flux. In the case of an incident heat flux increase, the time constant shortens with the increase in the incident heat flux and the decrease in the air flow rate. In this case, the effect of the incident heat flux and air flow rate on the time

constant are of the same order of magnitude. For all investigated cases, the effect of the air flow rate on the time constant is more pronounced in the 6.8×10^{-3}–7.7×10^{-3} $m^3 s^{-1}$ range. The observed inconsistencies in the observed tendencies are due to the experimental procedure. The manual positioning of the shutter and large time step of the acquisition system made it impossible to accurately correlate the measurement results with the moment of the step change in the incident heat flux. The obtained results indicate that the variation of the time constant values from the average in the power plant conditions will not exceed $\pm 10\%$.

CONCLUSION

The proposed 'clean' heat flux-meter is efficiently cooled by the air stream at the investigated air flow rates. The radial temperature difference in the receiving disc is linearly dependent on the incident heat flux. The dependence of the radial temperature differences on the air flow rate is evident, but it does not result in significant variations in the flux-meter signal caused by the air flow rate instabilities in real power plant boiler environments. For air flow rates higher than 16.6 $m^3 h^{-1}$, the temperature field in the receiving disc can be considered circumferentially uniform. The circumferential displacement of the peripheral thermocouple from the design position does not significantly affect the accuracy of the measurements. The 'clean' heat flux-meter can be calibrated accurately with the developed numerical model. The dynamic response of the 'clean' heat flux-meter to changes in the incident heat flux is good. All changes in heat transfer relevant to the monitoring of ash deposits in in-site conditions will be registered by the developed 'clean' heat flux-meter.

REFERENCES

1. D. Savic, N. Afgan, V. Jovic, Lj. Jovanovic, S. Markovic and P. Pavlovic, Effect of ash deposit on heat transfer performance in pulverized lignite fired boilers. In *Future Energy Production*. Hemisphere, Washington, DC (1976).
2. B. Brajuskovic, M. Matovic and N. Afgan, A heat flux-meter for ash deposit monitoring systems—I. Ash deposit prevention, *Int. J. Heat Mass Transfer* **34**, 2291–2301 (1991).
3. A. A. Ots, *Procesi v Parogeneratorah pri Szhiganii Slancev i Kansko Achinski Uglei*. Energia, Moscow (1977).
4. A. A. Ots and H. H. Aro, The mechanism of fouling steam generator surfaces under the combustion products of solid fuels. In *Fouling and Corrosion in Steam Generators* (Edited by D. Savic and I. Opik), pp. 29–41. IBK Vinca, Belgrade (1980).
5. A. G. Blokh, *Heat Transfer in Steam Boiler Furnaces*. Hemisphere, Washington, DC (1988).
6. S. B. H. C. Neal, E. W. Northower and R. J. Preece, The measurement of radiant heat flux in large boiler furnaces—II. Development of flux measuring instruments, *Int. J. Heat Mass Transfer* **23**, 1023–1031 (1980).
7. P. Radovanovic, B. Repic and B. Arsic, Investigation of steam blower system efficiency at Tuzla power plant (in Serbo-Croatian), IBK-ITE No. 621, Boris Kidric Institute, Vinca-Belgrade. (1984).
8. W. Clay and I. S. Davidson, Heat flux-meters in furnace boilers to monitor slag deposition, *Proc. Symp. on Thermal and Temperature Measurements in Science and Industry*, pp. 195–211. IMECO, Liverpool (1987).
9. A. K. Chambers, J. R. Wynnyckyj and E. H. Rhodes, Development of a monitoring system for ash deposits on boiler tube surfaces, *Can. J. Chem. Engng* **59**, 230–235 (1981).
10. M. Vrhovac and N. Afgan, A finite element model for heat conduction and thermoelastic stresses in screen tubes, *Proc. Symp. on Numerical Problems for Non-linear Problem* (Edited by C. Taylor, D. R. J. Owen and E. Hinton), pp. 937–950. University of Swansea, Swansea, U.K. (1987).
11. N. Afgan, B. Brajuskovic, M. Vrhovac and P. Radovanovic, Continual control of pipelines and boiler tubes (in Serbo-Croatian), *Elektroprivreda* **40**(7–8), 31–43 (1987).
12. B. S. Petuhov and L. T. Roisen, Obobschenie zavisimosti dlia teploodachi v trubah kolcevogo sechenia, *Teplofiz. Visokih Temp.* **12**(3), 565–569 (1974).
13. E. L. Crow, F. A. Davis and M. W. Maxfield, *Statistic Manual*. Dover, New York (1960).
14. P. Pavlovic, Development of boiler tube thermal load measurement method, M.Sc. Thesis, Belgrade University, Belgrade, Yugoslavia (1974).
15. A. V. Luikov, *Heat and Mass Transfer*. Mir, Moscow (1980).
16. E. I. Kazantsev, *Industrial Furnaces*. Mir, Moscow (1977).
17. F. Richter, *Physikalishe Eigenshaften von Stahlen und ihre Temperaturabhaengigkeit*. Verlag Stahleisen, M.B.H., Dusseldorf (1982).
18. R. Siegel and J. R. Howel, *Thermal Radiation Heat Transfer*. McGraw-Hill/Kogakusha Ltd, Tokyo (1972).
19. N. Afgan, P. Radovanovic and B. Brajuskovic, Effect of two-phase natural circulation distortion on tube failure in steam boilers, *Heat Transfer Engng* **8**(4), 58–63 (1987).
20. A. V. Luikov, *Teoria Toploprovodnosti*. High School, Moscow (1957).

UN FLUXMETRE THERMIQUE POUR DES SYSTEMES AVEC DEPOT DE CENDRE—II. CARACTERISTIQUES DU FLUXMETRE "PROPRE"

Résumé—On présente les caractéristiques d'un fluxmètre thermique "propre" refroidi par air et protégé contre le dépôt de cendre. La différence radiale de température permanente à travers le disque récepteur du fluxmètre est obtenue numériquement par la méthode des éléments finis et mesurée expérimentalement. On étudie l'uniformité circonférentielle du champ de température et la réponse dynamique du fluxmètre à un changement échelon du flux incident. Les données expérimentales et les résultats numériques indiquent que la différence de température radiale dépend linéairement du flux radiatif incident. On obtient aussi le signal en fonction du débit d'air. A toutes les conditions de régime permanent et de débits d'air les plus élevés, le champ de température du disque récepteur peut être considéré comme circonférentiellement uniforme. La réponse dynamique du fluxmètre thermique est satisfaisante.

EIN WÄRMEFLUSSMESSGERÄT FÜR SYSTEME ZUR ÜBERWACHUNG DER ASCHEABLAGERUNG—II. CHARAKTERISTIKEN DES "SAUBEREN" WÄRMESTROMDICHTEMEßGERÄTES

Zusammenfassung—Die Charakteristiken eines "sauberen" Wärmestromdichtemeßgerätes werden vorgestellt, das von einem Luftstrom gekühlt und gleichzeitg von ihm gegen Ascheablagerung geschützt wird. Für einen stationären Zustand wird die radiale Temperaturdifferenz über die Empfängerscheibe mit einem Finite-Elemente-Verfahren berechnet und außerdem gemessen. Weiterhin wird für den stationären Zustand die Gleichmäßigkeit des Temperaturfeldes am Umfang und das dynamische Verhalten des Meßgerätes bei einer Änderung des einfallenden Wärmestroms untersucht. Die experimentell und numerisch ermittelten Ergebnisse zeigen, daß die radiale Temperaturdifferenz linear vom einfallenden Wärmestrom abhängt. Außerdem ergibt sich das Signal in Abhängigkeit vom Luftvolumenstrom. Im stationären Zustand und bei großen Luftströmen kann das Temperaturfeld des Empfängers in Umfangsrichtung als konstant angenommen werden. Das dynamische Verhalten des Wärmestromdichtemeßgerätes ist zufriedenstellend.

ИЗМЕРИТЕЛЬ ТЕПЛОВОГО ПОТОКА В СИСТЕМАХ КОНТРОЛЯ ОТЛОЖЕНИЙ ЗОЛЫ—II. ХАРАКТЕРИСТИКИ ИЗМЕРИТЕЛЯ "ЧИСТОГО" ТЕПЛОВОГО ПОТОКА

Аннотация—Представлены характеристики охлаждаемого воздушным потоком и защищенного от образования отложений золы измерителя "чистого" теплового потока. Методом конечных элементов определена численно, а также измерена экспериментально стационарная радиальная разность температур на воспринимающем диске измерителя. Кроме того, исследуются однородность стационарного температурного поля воспринимающего диска по окружности и динамическая характеристика измерителя при ступенчатом изменении падающего теплового потока. Экспериментальные данные и численные результаты указывают на то, что радиальная разность температур линейно зависит от падающего теплового потока. Получена также зависимость сигнала от скорости воздушного потока. В условиях стационарного режима и при высоких скоростях воздушного потока температурное поле воспринимающего диска может считаться однородным по окружности. Динамическая характеристика измерителя теплового потока является удовлетворительной.